Frontal Waves Upstream of a Diabathic Blocking: A Model Study

LIE-YAUW OEY * AND PING CHEN

Department of Civil and Ocean Engineering, Stevens Institute of Technology, Hoboken, New Jersey

(Manuscript received 2 May 1990, in final form 29 April 1991)

ABSTRACT

A time-dependent, three-dimensional primitive-equation model is used here to study meanders that develop upstream of a western boundary current along a continental slope blocked by a diabathic topographic feature. It is found that episodic, large-amplitude meanders and shelfward intrusions occur at upstream distances, which coincide approximately with the topographic standing wavelength. In addition to its potential applications to other problems of front–topography interaction, the phenomenon may be relevant to branching and eddy intrusions of the Kuroshio southwest of Kyushu, Japan, and to the initiation and amplification of Gulf Stream meanders upstream of the "Charleston Bump," a topographic hump on the continental slope of the U.S. South Atlantic Bight.

1. Introduction

Observations indicate that the Gulf Stream (GS) along the continental slope of the South Atlantic Bight (SAB; see, e.g., Bane 1983) and the Kuroshio (KU) along the East China Sea (ECS; Sugimoto et al. 1988) continental slope develop instabilities and meanders. Numerical models (Orlanski and Cox 1973; Chao and Kao 1987; Oey 1988) suggest that the instabilities are baroclinic. While models with no bottom slope (e.g., Oey 1988) give realistic-looking meanders, inclusion of a continental slope gives less intense, small-amplitude meanders (Orlanski and Cox 1973). One objective of the present study is to investigate, through modeling, how topographic irregularities can induce finite-amplitude meanders more in accord with observations. There may be other mechanisms that can conceivably trigger meanders—transport variations by winds, for example. Topographic perturbations are, to us, more primitive and should be addressed. Specifically, we study the effects of deflection and blocking on a western boundary current (WBC) by a topographic feature on the continental slope. Two examples are: deflection of the Gulf Stream by the Charleston Bump in the South Atlantic Bight and blocking of the Kuroshio along the East China Sea continental slope by the island of Kyushu, Japan (Fig. 1). The latter is studied in this paper, because it is also a limiting case of a seamount that rises above the sea surface. The blocking of the front by a seamount or "bump" involves somewhat different dynamics and will be discussed in a later paper.

The Kuroshio flows along the ECS continental slope/shelfbreak from north of Taiwan (25°N, 122°E) to about 300 km southwest of the island of Kyushu, Japan (29°N, 127°E), where it deflects eastward (Fig. 1). The deflection is due in part to diverging bottom topography, which in a region extending southwestward for about 300 km from Kyushu shows bottom shoaling with depths of less than 1000 m. We will henceforth refer to this bottom feature as the Kyushu shoal. However, observations suggest that not all of the Kuroshio water is deflected seaward. Part of the Kuroshio water branches shelfward to become the Tsushima Current and the Yellow Sea Warm Current (Nitani 1972; Guan 1983), as we schematically show in Fig. 1.

The schematic in Fig. 1 tends to give the impression that shelfward branching of the Kuroshio is continuous. Recent studies suggest, however, that the branching is made up of cumulative intrusions, across the shelfbreak, of eddies from the Kuroshio (Huh 1982; Ichiye 1984; Muneyama et al. 1984). Huh's satellite images show that warm eddies, which presumably are shed from the Kuroshio, are often present southwest of Kyushu. Similar eddies are also seen in the images presented by Muneyama et al., who further supported their findings with hydrographic and current meter measurements.

While the present research is motivated by these specific observations, we raise the following questions of relevance to the studies of WBC/shelf interactive dynamics in general. (i) Since topographic Rossby

* Also affiliated: Program in Atmospheric and Oceanic Science, Forrestal Campus, Princeton University, Princeton, New Jersey.

Corresponding author address: Dr. Lie-Yauw Oey, Atmospheric and Oceanic Sciences Program, Sayre Hall, Forrestal Campus, Princeton University, Princeton, NJ 08544.

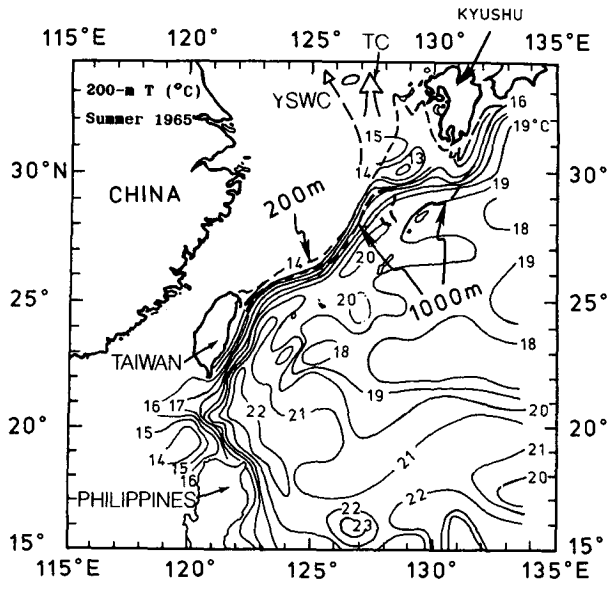

FIG. 1. Temperature contours at 200-m depth showing the Kuroshio front along the East China Sea continental slope (from Nitani 1972). The 200-m and 1000-m isobaths are also shown. YSWC: the Yellow Sea Warm Current; TC: the Tsushima Current.

waves propagate against the generally parabathic (i.e., parallel to isobath) flow of the WBC front, could wave–frontal flow interaction produce sources of instabilities *upstream* of a diabathic (i.e., diagonal to, or cross, isobath) topographic irregularity? (ii) Can increased eddy activity upstream of the irregularity be of sufficient intensity as to modify or even determine the circulation and water-mass balance of the adjacent shelf? (iii) What is the dynamics of intrusions on the continental shelf? (iv) What is the effect on shelfwide circulation of the WBC forcing at the shelfbreak? (v) Can this forcing be important in the nearshore regions where circulation induced by winds, tides, and estuary-borne buoyancy often dominate? The present study focuses on items (i) and (ii). The other items will be addressed in a separate study.

The topographic standing wave, which would result upstream of a blocking, typically has a wavelength of 150–200 km, approximately equal to the wavelength of a propagating frontal meander (the meander wavelength is about $2\pi R_0 \approx 180$ km, where $R_0 \approx 30$ km is the baroclinic Rossby radius of deformation). Large amplitude can be expected to develop, therefore, if the crest (shelfward-most excursion) of the meander coincides with the standing wave crest. Thus, one expects intermittant shelfward intrusions near the (blocking) wall, as well as near multiples of 150–200 km upstream of the wall, at periods coincident with that of the propagating meanders, which is about 10–20 days. The preference locations of these intrusions, as well as their periods, are noteworthy consequences of these arguments and are ones that we explore here by means of a numerical model. For convenience, we loosely label the phenomenon as *meander resonance.*

While the two conditions for meander resonance, blocking and sloping topography, exist along the ECS shelfbreak, observations there are not extensive enough to provide clues as to the structure of the KU front, its meanders, and also whether or not the front is sufficiently barotropic to support topographic waves. We looked instead, then, at the GS front along the SAB continental shelfbreak, where observations are more extensive. Here, meanders on the inshore portion of the stream are shallow features ($\approx$100 m) hugging close to the shelfbreak (Lee and Atkinson 1983). Both the mean and fluctuating alongfront velocities show significant baroclinicity and the fluctuations are vertically coherent. Despite significant vertical shears, the mean current is unidirectional (i.e., predominantly northward) throughout the water column (Richardson et al. 1969). Moreover, farther inshore over the outer shelf, the currents become more barotropic. These features of the GS conform with what we envision as the type of parabathic frontal flow that can give rise to amplified meanders upstream of a blocking.

Propagating frontal meanders have been observed from satellite data for the KU along the ECS shelfbreak (Sugimoto et al. 1988). The meanders are similar to those found in the SAB, especially along their inshore edges over the shelfbreak. Moreover, the KU appears to be more barotropic (Worthington and Kawai 1972). Thus, our hypothesis for meander resonance may be relevant to the KU eddy intrusions upstream of the Kyushu blocking. In the following, we perform time-dependent, three-dimensional model experiments to support the hypothesis.

The outline of the paper is as follows. Section 2 gives the model formulation. We take as observed features blocking processes, which occur southwest of the Kyushu Island along the ECS continental slope, and configure a model domain that incorporates the gross features of the region—a spunup WBC, the island and continental slope, for examples, without however duplicating its details. In section 3 we discuss the spinup calculation, as well as the mean fields. Temporal variabilities are presented in section 4 in which we first show the existence of meander amplification for an experiment with simple blocking and contrast it with the results of other experiments without blocking, as well as those that include topographic features (bottom humps). In section 5 we discuss mean transports over the shelf and show that transport variation across the model Korea Strait, in particular, is strongly related to transport variation across the shelfbreak southwest of Kyushu; the latter, in turn, varies with the periods of eddy intrusions from the model WBC. The paper ends with a concluding summary/discussion in section 6.

2. The model

a. The model domain

The model domain (Fig. 2) is 2200 km east–west and 2400 km north–south. It consists of a continental shelf, which represents the ECS, in the midlatitude of its western portion, 50–100 m deep, approximately 140 km east–west, and 1000 km north–south. The ocean depth increases eastward from 100 m in the outer shelf to 4000 m in the deep ocean, and the depth transition is over a continental shelfbreak/slope of about 250 km wide. The horizontal grid spacing is variable in x, with $\Delta x = 20$ km over the shelf and the western half of the ocean basin, increasing linearly to $\Delta x = 200$ km near the eastern wall, and $\Delta y = 30$ km (Fig. 2). The vertical grid distribution across the shelf and into the deep ocean is given in Fig. 3a. The parallel isobaths along the shelfbreak/slope are interupted by an east–west wall in the northern part of the shelf, representing the southern coast of Kyushu. Both the southern and northern ends of the continental shelf connect through straits to "mini"-ocean basins in the southwest and northwest, representing the South China Sea and the Japan Sea, respectively. For convenience, the southern strait will be referred to as the Taiwan Strait, while the northern strait the Korea Strait. The opening that connects the southern minibasin to the main ocean basin is referred to as the Luzon Strait. The northern minibasin serves a more important purpose for the present study, because it is where intrusive transport from the Kuroshio ultimately flows into. It is of depth 4000 m, east–west width 600 km, and north–south length 500 km. It connects to the main ocean basin through an opening at its northeastern wall. The southern basin is of depth 500 m, east–west width 500 km, and north–south length 1100 km. It serves as a "buffer zone" so that any WBC branching through the Luzon Strait and into the Taiwan Strait can be more realistically accounted for.

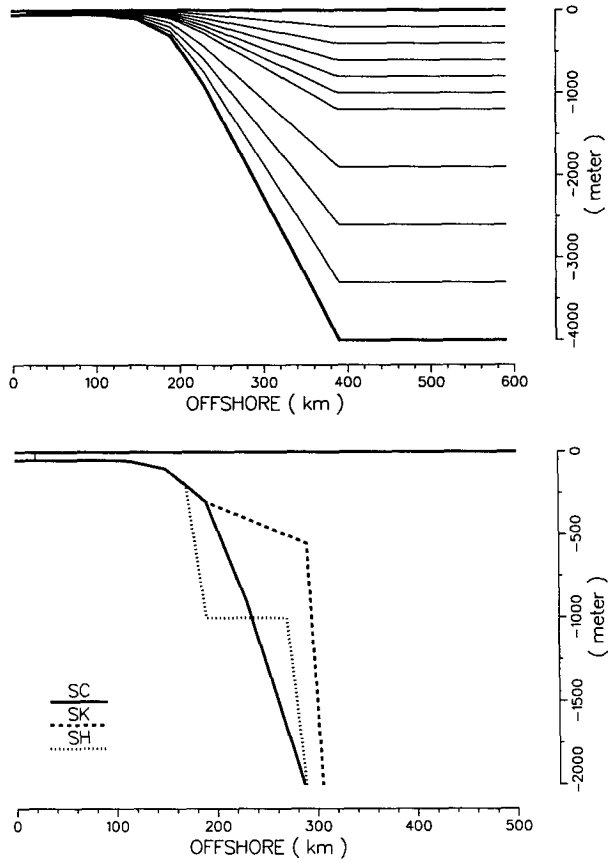

FIG. 3. (a) The model's vertical grid distribution across the shelf, slope, and the deep ocean. (b) The different cross shelf/slope distributions of topography used for experiments *SC*, *SH*, and *SK*. For *SK*, the changed topography is over the shaded region shown in Fig. 2.

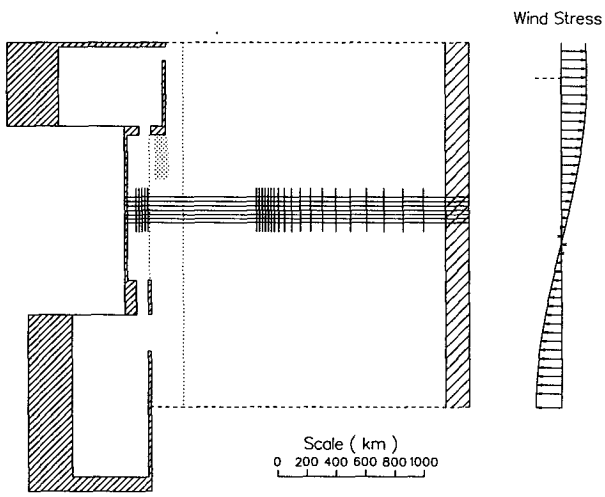

FIG. 2. The model domain used in the experiments *SC*, *SH*, and *SK* (see Table 1). The 200-m isobath at the shelfbreak, as well as the 4000-m isobath farther offshore, are shown as dotted lines. The shaded region south of the blocking wall is where the bottom bump is put in for experiment *SK*. The zonal wind stress used is shown on the right-hand panel. Maximum arrow is 0.25 N m^{-2} and the zero-curl latitude is marked by a dashed line. The grid distribution used in the main region of interest is also shown.

Rather than mimicking all detailed bathymetry of the continental shelf and its adjoining seas, we choose to extract what is the most important for the study of the blocking dynamics: sloping topography and the Kyushu coast. The present study is therefore what Chao and Kao (1989) termed as being "process-oriented," seeking to identify the dominant mechanism for meander development and shelfward eddy intrusions, "in the hope that it may be relevant to sea truth." For convenience, we freely use the name "Kyushu" to denote the blocking island.

A model domain with open boundaries could have been designed through which inflow and outflow

transports can be specified (e.g., see Thompson and Schmitz 1989). While schemes can be devised to force a western boundary current, there is always the uncertainty with regard to proper treatment of meanders and eddies that may cross boundaries. We chose to avoid these and opted for a closed basin in which a western boundary current can be spun up by specifying the wind-stress curl. If meanders and eddies develop in the model, they are not triggered by errors that might be produced at open boundaries.

We also wish to demonstrate that shelfward eddy transport south of Kyushu is correlated with transport variation into the northern minibasin through the Korea Strait, and that this correlation is statistically valid after the model has reached a quasi-equilibrium state. By setting up a basin-scale model, some degree of realism is introduced into the statistics of the calculation.

b. *The governing equations*

We solve in the model the finite-difference analog of the following set of (primitive) equations

$$\nabla \cdot \mathbf{u} + w_z = 0 \tag{1a}$$

$$u_t + \mathbf{u} \cdot \nabla \mathbf{u} + w u_z + f \mathbf{k} \times \mathbf{u} = -\nabla p/\rho_0 + (K_M u_z)_z + \nabla(A \nabla u) \tag{1b}$$

$$\rho g = -p_z \tag{1c}$$

$$e_t + \mathbf{u} \cdot \nabla e + w e_z = (K_H e_z)_z + \nabla(A \nabla e) \tag{1d}$$

$$\rho = \rho(T, S) \tag{1e}$$

where x, y, z form a right-handed Cartesian coordinate system with positive x eastward, positive y northward, and z positive upward (unit vector $\mathbf{k}$), with $z = 0$ at the mean free surface. Here t is the time; ∇ is the horizontal gradient operator, $\mathbf{u}$ is the horizontal velocity vector with components u and v in the x and y directions, w is the vertical component of velocity, ρ_0 is a (constant) reference density, p and ρ are deviation pressure and density (i.e., the hydrostatic pressure associated with ρ_0 has been subtracted from the system); e denotes either temperature T or salinity S, which are related to ρ through the equation of state (1e). For the present application, $e = T$ and S is set constant at 35‰. The model is on a beta plane centered at the 31°N latitude, so that

$$f = 7.5 \times 10^{-5} + 1.96 \times 10^{-11}(y - y_0)\ \mathrm{s}^{-1}, \tag{2}$$

where $y_0 = 1200$ km. The x, y axes are such that $x = 0$ is at the coast of the shelf and $y = 0$ at the southernmost boundary of the main ocean basin.

The horizontal viscosity/diffusivity coefficient, A, is specified so that it is $= 50\ \mathrm{m^2\ s^{-1}}$ over the shelf where $H = H_{\min} = 50$ m and increases with depth to a maximum of $350\ \mathrm{m^2\ s^{-1}}$ for $H \geqslant 1290$ m:

$$A = \begin{cases} 50 + 0.242\,(H - H_{\min})\ \mathrm{m^2\ s^{-1}}, \\ \qquad\qquad H_{\min} \leqslant H \leqslant 1290\ \mathrm{m} \\ 350\ \mathrm{m^2\ s^{-1}}, \quad 1290\ \mathrm{m} < H. \end{cases} \tag{3}$$

The precise form of the variation is not expected to be important, however, and the main purpose of A is to damp grid-scale numerical noise. Its value is chosen small enough that the WBC is mildly inertial with the Reynolds number, $\mathrm{Re} = V_a W/A \approx 60$, where $W \approx 50$ km is half-width of the WBC, and $V_a \approx 0.35\ \mathrm{m\ s^{-1}}$ the northward velocity averaged over the cross section of the WBC east of Taiwan, a section where the WBC enters the shelfbreak/slope.

The K_M and K_H are vertical eddy viscosities and diffusivities, respectively. These are computed using the Mellor–Yamada turbulence closure model as in Oey et al. (1985). We believe that stratification dependency of turbulent mixing is necessary for proper accounts of intrusion processes on the shallow shelf and that the higher computing overhead is justified.

Other details of the numerical method, which include leapfrog time differencing with split external/internal modes, horizontal spatial differencing that conserves linear and quadratic quantities, vertical σ coordinates in implicit form with a tridiagonal solver, etc., are given in Blumberg and Mellor (1983) and Oey et al. (1985). For the present application, the time step for the three-dimensional calculation (the internal mode) is 1200 sec and is 40 sec for the two-dimensional depth-averaged calculation of transports and surface elevation.

c. *The boundary conditions*

The normal component of momentum and heat fluxes are zero at all horizontal walls. The tangential velocities are set zeros at all horizontal walls except those at the northern and southern walls, where free-slip conditions are applied. At the ocean floor, heat flux is zero while momentum flux is balanced by frictional stress computed by matching the computed velocity nearest the bottom (u_b) with the logarithmic law of the wall. Thus,

$$\left.\begin{aligned} (K_H T)_{z_n} &= 0 \\ (K_M u)_{z_n} &\sim C_D |\mathbf{u}_b| \mathbf{u}_b \end{aligned}\right\} \quad \text{as} \quad z \to -H, \tag{4}$$

where z_n is normal to boundary, $C_D = \max\{2.5 \times 10^{-3}, \mathrm{k^2/ln}[(H + z)/z_r]\}$, $k = 0.40$ is von Kármán's constant, H is local depth, and $z_r = 1$ cm is the roughness height.

We spin up the ocean using a zonal wind stress that varies with latitude, as shown on the right-hand panel of Fig. 2. To simplify interpretations of flow dynamics in the WBC/shelf, the wind stress is applied only over the deep ocean $x > 350$ km. The wind therefore serves

solely to create midocean Svedrup transport and northward return flow in the western boundary layer along the shelfbreak/slope. Based on observations in the SAB (see, e.g., papers presented in *J. Geophys. Res.*, Vol. 88, 1983), WBC/shelf interaction processes depend on whether the shelf is stratified (summer) or well mixed (winter). The computed transports over the shelves and straits will likely be different in both cases. We believe that the well-mixed scenario is simpler to understand. In order to produce vertical mixing without complicating the solutions with wintertime strong wind cycles, heat flux boundary conditions were applied at the surface. This way we introduce a little realism into the calculation. Also, good satellite images (e.g., see Huh 1982) from which our "empirical" hypothesis of the blocking problem was originally derived (see the Introduction) are usually taken during cloudless days in winter. Thus, surface cooling of -300 W m^{-2} was applied over the shelf north of the midsection of Taiwan Strait and in the northern minibasin and heating over the eastern portion of the main basin ($x > 350$ km), such that the summed heat input/output is zero. It should be emphasized that, even with cooling, the shelf condition is not representative of the winter because wind-induced circulation is excluded. This is advantageous for our purpose, however, since over the model shelf and shelfbreak, responses can be studied purely as a result of forcing by the WBC.

The model ocean is initially quiescent and vertically stratified:

$$\left.\begin{aligned} \mathbf{u} &= 0 \\ T &= 10°\text{C} \end{aligned}\right\} \quad \text{over the shelf where } H < 100 \text{ m}$$

and

$$T = \begin{cases} 25°\text{C}, & z \geqslant -50 \text{ m} \\ [25 + 22(z + 50)/1450]°\text{C}, & \\ & -50 \text{ m} > z \geqslant -1500 \text{ m} \\ 3°\text{C}, & -1500 \text{ m} > z. \end{cases} \quad (5)$$

Wind and surface heating/cooling are then applied. The calculation continues until it has reached a quasi-steady state with a well-defined WBC along the shelfbreak and a cooled well-mixed shelf.

Four experiments will be presented (Table 1). Experiment *SC* is a spinup calculation with model configurations and parameters specified as discussed above. It also serves as a control experiment. In *SH*, year 5 of the spunup solution from *SC* is perturbed by gradually flattening the continental slope south of Kyushu to a uniform depth of 1000 m over a period of 10 days, and the calculation is continued for another N days for analysis. In *SK* the *SC* solution is perturbed by introducing a topographic hump south of Kyushu, also over a 10-day period. The different cross-shelf/cross-slope distributions of topography used in these experiments are shown in Fig. 3b. Finally, an experiment with no blocking, *SO*, is conducted, spun up from rest and reducing Δy from 30 km in *SC* to $\Delta y = 20$ km. This reduction in Δy is to increase resolution for future experiments with seamounts and does not affect conclusions to be derived in the present study. The value of N is 185 for *SH* and is 365 for *SK*. For *SC* and *SO* it is the last 365 days of a 6-year run that is analyzed.

TABLE 1. List of experiments conducted.

SC	The spinup and control experiment
SH	The flat continental slope experiment
SK	The Kyushu shoal experiment
SO	The experiment with no blocking

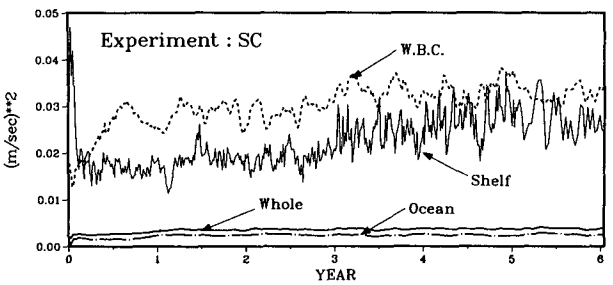

FIG. 4. Experiment *SC*: Kinetic energies averaged over four different regions of the model domain.

3. The model results: The spinup and the mean field

Results for experiment *SC* only are shown here. Intercomparisons of results from different experiments will be given in section 4 on discussion of the temporal variabilities.

a. Establishment of the WBC

Figure 4 gives time series of kinetic energy (KE) spatially averaged in four different regions over the model domain: the main basin (labeled ocean), the WBC, the shelf, and their sum (labeled whole). The initial temperature front, located approximately over the slope/shelfbreak [see Eq. (5)], gives rise to an initial PE (potential energy), which drives the shelf KE in times of O(days). A peak mean current (predominantly alongshelf) magnitude of about 0.2 m s^{-1} is produced over the shelf. At later times, the shelf KE settles to lower values—the shelf current now being driven by the developing WBC.

The development of the WBC (especially near its surface) during the initial times is also influenced by the initial PE of the front over the slope/shelfbreak. This explains the O(days) increase in KE over the WBC.

Barotropic adjustment by the wind then ensues in times of O(10 days) in which the mean alongfront current rises to about 0.15 m s^{-1}. The WBC KE continues to rise as a result of the baroclinic adjustment, in times of about 3 years. These time scales correspond approximately to the times for the respective barotropic and first baroclinic Rossby waves to cross the main basin. From t = 4–6 years, the WBC curve oscillates

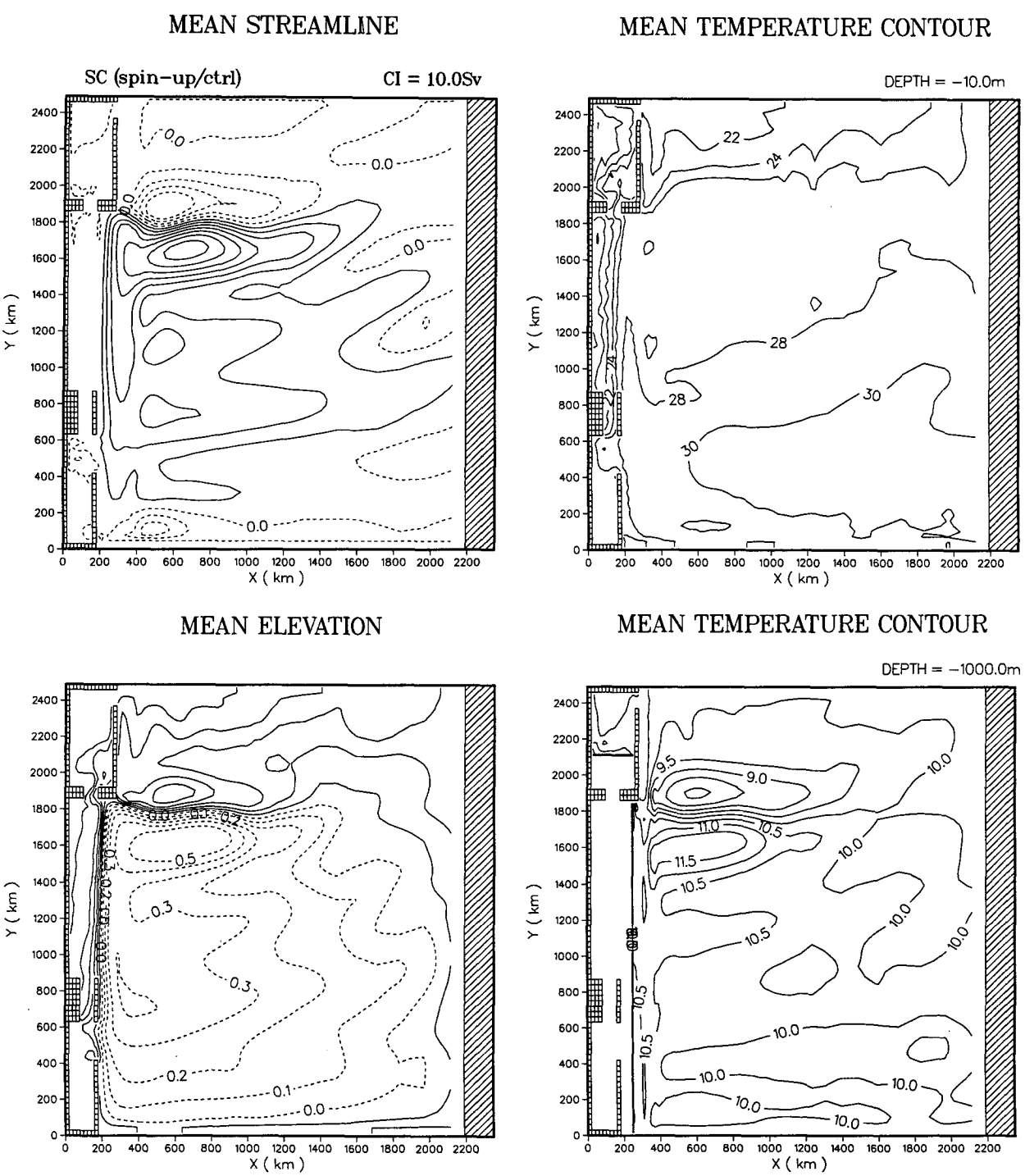

FIG. 5. Experiment *SC*: 1-yr mean (a) streamfunction, (b) elevation, (c) temperature at z = −10 m, and (d) temperature at z = −1000 m.

about a mean trend that is nearly flat. The same thing can be said about the shelf curve from about $t = 4.5$ through 6 years. We assume, therefore, that the system has reached quasi-equilibrium state, and that meaningful statistics can be obtained for the analyses of the WBC and shelf dynamics.

Over the deeper ocean the influence of the initial front is much less, but not entirely nil, especially since the volume used to define deeper ocean actually includes a little of the eastern edges of the WBC. The deep-ocean KE seems to stabilize in about 4–5 years.

Figure 5 shows the one-year (from 5 to 6 years, saved every 1 day) averaged streamfunction, elevation, and temperatures at $z = -10$ m and $z = -1000$ m. For clarity, the minibasins north and south of the shelf have not been plotted to scale. The width of the WBC is about 100 km and its transport is about 30 Sv (1 Sv $\equiv 10^6$ m^3 s^{-1}), overspun in comparison to that driven by the specified wind-stress curl, which would give approximately 23 Sv; the system is therefore mildly nonlinear. Southward drift prevails in the ocean interior. There is a Fofonoff-type cyclonic gyre near the southern boundary, formed because of the free-slip condition there, but the flow is otherwise self-confined and should not affect the WBC/shelf dynamics. The elevation and temperature contours show much the same large-scale features as the streamfunction plot. Note that the WBC leaves the coast at the reversed L corner made by Kyushu and the outer eastern wall of the northern minibasin, rather than at the zero wind-curl latitude some 400 km farther north. For experiment *SK* (not shown), overshooting occurs and the separation is near the zero wind-curl latitude. The reason for this difference appears to be related to the strength of eastward flow at Kyushu; that is, the mean flow for *SC* is more inertial than for *SK*. This is an interesting result, which deserves a separate more complete study.

Figure 6 shows vertical (xz) section contours of the mean temperature and meridional velocity across a section where the WBC just enters the shelf region (i.e., at $y \approx 900$ km in Fig. 5). The WBC hugs close to the continental slope/shelfbreak and the computed profiles are similar to published observations (e.g., Worthington and Kawai 1972; Lee and Waddell 1983; Oey et

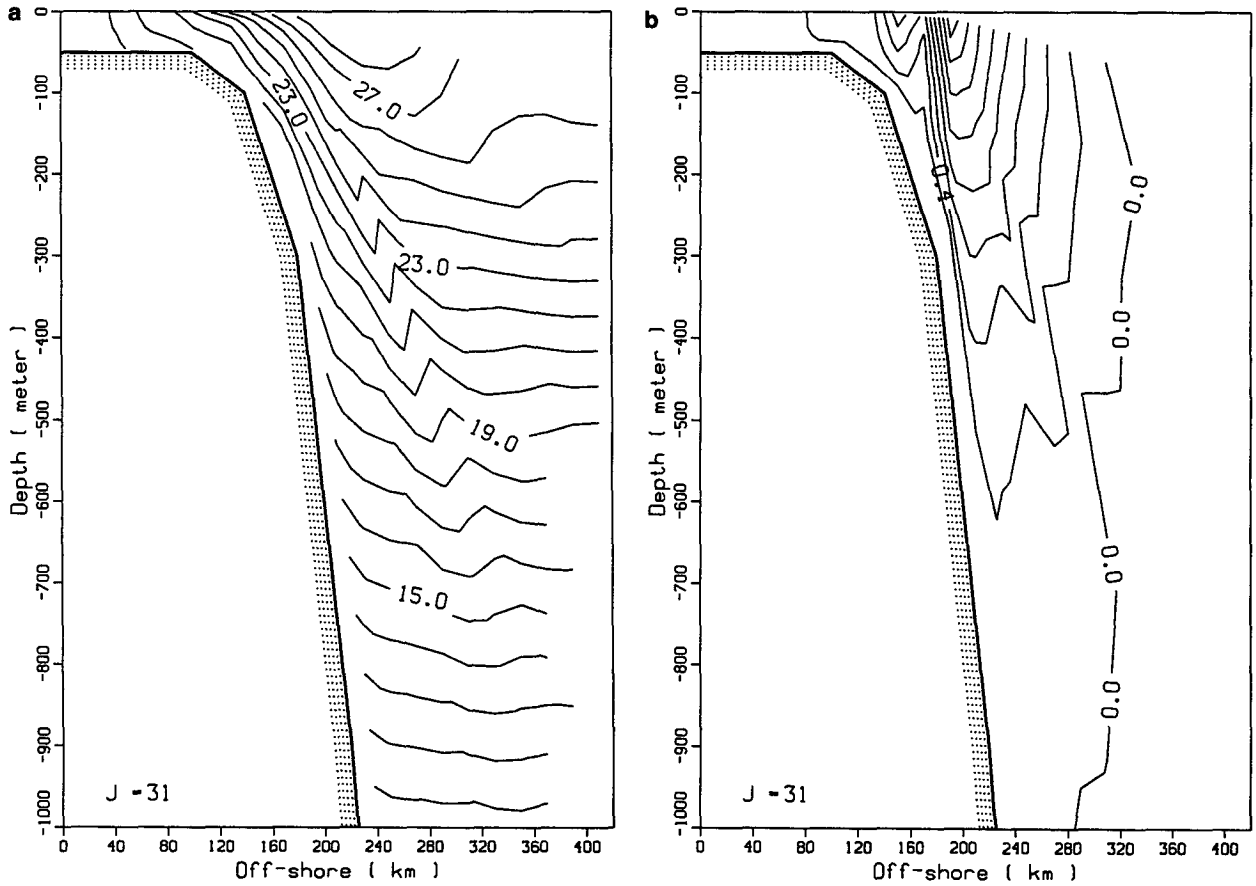

FIG. 6. Experiment *SC*: one-year mean cross shelf/slope and depth contours of (a) temperature and (b) meridional velocity at a section just north of Taiwan.

al. 1987). The establishment of a WBC with fairly realistic features is important and well worth the efforts spent in driving the Svedrup interior flow.

b. Circulation in shelf and local seas

Over the shelf, Fig. 5b shows a northward dip in elevation of gradient of about -10^{-7}, or -10 cm in 1000 km, due entirely to the presence of the WBC. This value agrees fairly well with that reported by Blanton et al. (1989) for the GS in the SAB. In Fig. 6 the water is well mixed over the shelf. Moreover, shelfward intrusion is evident here with the establishment of a subfrontal feature over the outer shelf, at $x \approx 150$ km. These features are typical of what has been observed in the SAB during winter (Oey 1986; Oey et al. 1987; Atkinson et al. 1989).

In the southern minibasin (the South China Sea) the mean elevation and near-surface temperature fields show westward intrusion of the WBC water. Most of the intruded water rejoins the WBC in a rather tight anticyclonic turn, however, and about 2–3 Sv (details in section 5) flows into the main shelf through the southern strait (the Taiwan Strait). A larger scale cyclonic gyre in the (southern) basin is also seen in the mean streamfunction plot. These results, from a geometrically highly idealized model, are in broad agreements with available observations (Nitani 1972; Shaw 1989).

The circulation pattern in the northern basin is, in the model, purely driven by the WBC intrusion through the northern strait (the Korea Strait). Its broad features, through-strait transport of about 4 Sv (details in section 5) and an anticyclonic turn of the intruded water as it flows into the basin, as indicated by the temperature and elevation plots, conform also with observations (Moriyasu 1972; Miita and Kawatate 1986).

These descriptions of the mean fields in the southern and northern minibasins are necessarily brief as our main focus is with the WBC/shelf interactive processes. The model results in these local seas deserve further analyses, however.

4. The temporal variabilities

a. The spinup and control experiment SC: Frontal meanders and intrusions

We searched for northward-propagating frontal meanders in the computed near-surface temperature fields but instead found one or two specific locations along the shelfbreak/outer shelf where shoreward intrusions appeared to be predominant. Figure 7 shows an example of the temperature image, at $t = 1892$ days and $z = -30$ m, for the region that encloses the northern 600 km of the shelf and includes a portion of the WBC. A local coordinate system is adopted in which $y = 0$ is aligned with the southern coast of Kyushu. The light gray tone occupying approximately one-third of the image on the right side signifies the main core of the WBC with $T \geqslant 28°C$. The shelfbreak front (i.e., the inshore portion of the WBC front along the shelfbreak–outer shelf) is signified by the dark gray tone on which $T = 21°C$, and the region to its left is cooler shelf water. The shelfbreak front shows abrupt shelfward meander crests followed by more gradual seaward troughs, similar in shape to that described in Oey (1988). The largest crests at this instant are at locations shoreward of Kyushu, and at 150–200 km and 300–400 km upstream of Kyushu. There are eddies, which have pinched off or are about to pinch off, at these crests. On examination of one-years worth of images (by "watching" on a Sun workstation a color movie of the temperature field), we find that the crest at Kyushu is quasi permanent, while those at other locations grow and disappear with time. Thus, while pinched-off eddies are often found shoreward of these crests, the large crests themselves do not visually propagate along the front. Rather, the large meanders and pinched-off eddies tend to spread over the shelf. On the other hand, small-amplitude frontal waves do propagate along the slope/shelfbreak. As an example, this propagation is shown in Fig. 8 with contours of perturbation temperature, evaluated at $z = -100$ m along the shelfbreak (the 600-m isobath) from north of Taiwan to a region south of the northern minibasin, on a time and alongslope distance plane. The northward propagation speeds of these waves range from 0.5 to 0.7 m s^{-1}, which agree with values observed for the GS frontal waves along the SAB shelfbreak by Lee and Atkinson (1983). The temperature images suggest then that small-amplitude, propagating frontal waves amplify at specific along-shelfbreak locations. In the following an example is given in which a frontal wave along the shelfbreak was seen to amplify in time of O(days) into large amplitude shelfward meander.

Figure 9 shows four snapshots of the near-surface temperature contours from $t = 1894$ days though 1903 days at 3-day intervals. The domain again includes only the northern 600-km portion of the shelf, as well as part of the WBC. The shelfbreak front is here signified by the $T = 21°$–$25°C$ contour, and the $T = 23°C$ contour is highlighted by a thick dashed curve. At $t = 1894$ days, the $T = 21°C$ contour shows shelfward intrusion at about 300–400 km upstream of Kyushu. This is reminiscent of earlier meander amplifications at these locations, and the contour also shows an example of eddy detachment at location $y = -300$ km. The same contour also shows a small meander crest at $y = -200$ km, which at $t = 1897$ days has amplified shoreward. At this time, the $T = 23°C$ contour also shows amplification of a small meander crest at $y = -225$ km, which propagates downstream (see figures at $t = 1900$ and 1903 days), and at $t = 1903$ days there is indication that a warm eddy has detached. By $t = 1903$ days the

T = 21°C contour shows development of a large meander with an abrupt shoreward excursion at y = −230 km, followed by a gentler seaward meander that extends northward to y = −170 km. Within the context of the standing Rossby wave theory, the steady parabathic flow in the model would be over the sloping outer shelf/shelfbreak, and would correspond therefore to the inshore more barotropic portion of the WBC. On the other hand, an energy analysis similar to that in Oey (1988) indicates that the WBC meanders over the slope are produced predominantly by baroclinic instability. These results suggest that propagating frontal meanders produced by baroclinic instability can become phase-locked with the standing wave to produce a time-dependent, large-amplitude shoreward meander. A notable feature of this type of meander is that, during its entire amplification stage of O(10 days), it remains essentially stationary. We next present results that show that the locations of large meanders coincide with nodes of the topographic standing wave.

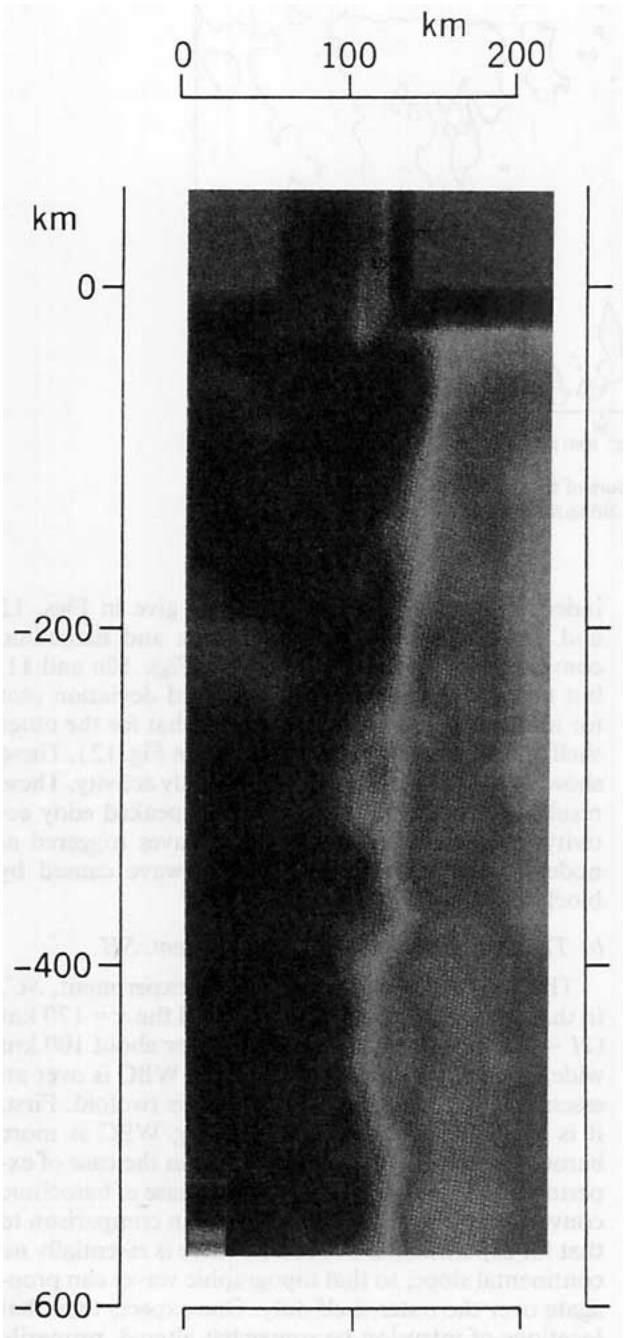

FIG. 7. Experiment *SC*: an image of the temperature field at t = 1892 days and z = −30 m, over the northern portion of the shelf and part of the WBC. The light gray tone occupying approximately one-third of the image on the right side signifies the main core of the WBC with $T \geq 28$°C. The shelfbreak front is signified by the dark gray tone on which T = 21°C, and the region to its left is cooler shelf water.

We attempted to look for the standing wave solution component in the mean temperature field but found only a rather weak signal (Fig. 5c). The reason is that the average of the computed field is not equivalent to the true steady state (e.g., see Pedlosky 1979) since intruded eddies tend to smooth out the temperature field over the outer shelf and shelfbreak. We therefore examined the eddy field instead in order to quantify that shoreward intrusions occur at specific locations. Figure 10a is a plot of the standard deviation of temperature averaged over the upper 25 m of the water column at two midshelf locations, x = 90 km (solid; local depth = 50 m) and x = 110 km (dash; local depth = 75 m), as functions of alongshelf distance. The alongshelf coordinate is from the northern tip of Taiwan (y = 0 km) to the southern coast of Kyushu (y = 1000 km). Upstream of Kyushu, peaked values are seen at three to four alongshelf positions: the first one shoreward of Kyushu ($y \approx$ 950 km), another one some 150–200 km farther upstream ($y \approx$ 730–830 km), and yet another one at about 400 km upstream of the first ($y \approx$ 500–550 km). There are also peaks farther upstream about 600 km and 800 km, which may also be manifestations of a standing-wave meander associated with the blocking. The peaks, in general, are caused either by warm eddies, which have pinched off from their respective parent crests farther offshore, or by the episodic shoreward spreading of the parent crests. The alongshelf locations of these peaks indicate, therefore, locations of amplified parent meanders along the shelfbreak. The upstream length scales for the first two peaks agree with the wavelength (and multiple thereof) of the standing wave, which for the model's slope over the outer shelf and shelfbreak gives a value of about 150–200 km. Figure 10b gives the same standard deviation plots for two locations farther offshore, x = 130 km (solid; local depth = 100 m), and x = 150 km (dash; local depth = 200 m). Here, only the peak at 150–200 km upstream of Kyushu stands out; those farther upstream and at Kyushu are barely discernible.

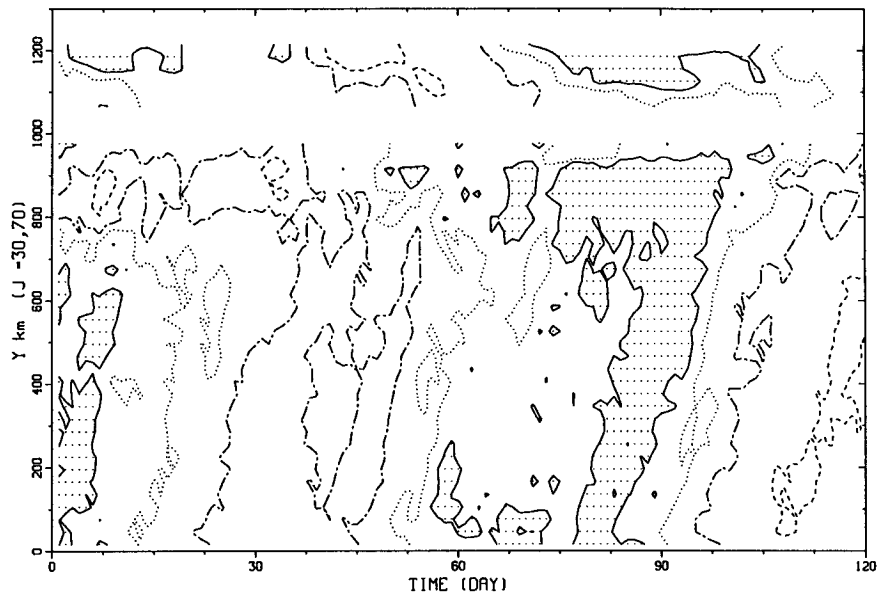

FIG. 8. Experiment *SC*: time–alongslope contours of the perturbation temperature at $x = 190$ km and $z = -100$ m. The water depth along this shelfbreak location is 600 m.

At Kyushu, a quasi-permanent meander exists and the peak-to-background ratio is weak for the offshore locations. Farther upstream (of the peak at 150–200 km), peaks are smoothed by propagating frontal waves, which are significant at the outer shelf and shelfbreak locations. It is seen that, moving northward along the shelfbreak at $x = 150$ km (Fig. 10b, dash), enhanced eddy activity does not occur until about 200 km upstream of the blocking. This region of enhanced eddy signal will be shown in section 5 to be related to significant shelfward transport of the WBC water.

One may argue that the peaks in Fig. 10 may not be sufficiently distinct to support the meander amplification hypothesis, since the peak-to-trough difference is only about 0.5°C, in comparison to an alongshelf mean of about 1.5°C. The reason for this small difference is that meanders, which amplify at a specific site, tend to spread over the shelf and hence contribute also to variabilities in the neighborhood, especially downstream of that site. To avoid this possible ambiguity, the cross-shelf eddy heat flux, $\int_{-H}^{0} -\overline{u'T'}\, dz$, along the shelfbreak was calculated. The result, in Fig. 11, shows peaks at alongshore locations (in particular, those at $y \approx 530$ km and $y \approx 800$ km) that coincide approximately with the peaks in Fig. 10. Moreover, since $\int_{-H}^{0} -\overline{u'T'}\, dz$ is a measure of the baroclinic conversion term (e.g., see Oey 1988), the peaks indicate sites of enhanced baroclinic instabilities—a result consistent with our hypothesis that meander amplification at the standing wave node is a result of enhanced baroclinic instability process.

Finally, to show that the aforementioned results are indeed caused by flow blocking, we give in Figs. 12 and 13 the same standard deviation and baroclinic conversion plots, respectively, as in Figs. 10b and 11, but now for experiment *SO* (standard deviation plot for midshelf locations are similar to that for the outer shelf and shelfbreak locations shown in Fig. 12). These show no special locations of peaked eddy activity. These results indicate that the locations of peaked eddy activity in *SC* are due to amplified waves triggered at nodes of the topographic standing wave caused by blocking of the WBC.

b. The flat continental slope experiment: SH

This case differs from the control experiment, *SC*, in that the bottom topography beyond the $x = 170$ km ($H = 300$ m) is constant at 1000 m for about 100 km wide, as shown in Fig. 3b. Thus, the WBC is over an essentially flat bottom. The purpose is twofold. First, it is expected that the corresponding WBC is more baroclinic. An energy analysis gives, in the case of experiment *SH*, a two- to threefold increase of baroclinic conversion of mean to eddy energies in comparison to that for experiment *SC*. Second, there is essentially no continental slope, so that topographic waves can propagate over the outer shelf only. One expects then that locations of intrusion be somewhat altered, primarily because the influence of Kyushu is now diminished. However, since the model's sloping outer shelf is interrupted by the shelfbreak and slope of the northern minibasin where water depth increases to 4000 m, this then becomes the dominant diabathic disturbance source upstream of which a topographic wave can form.

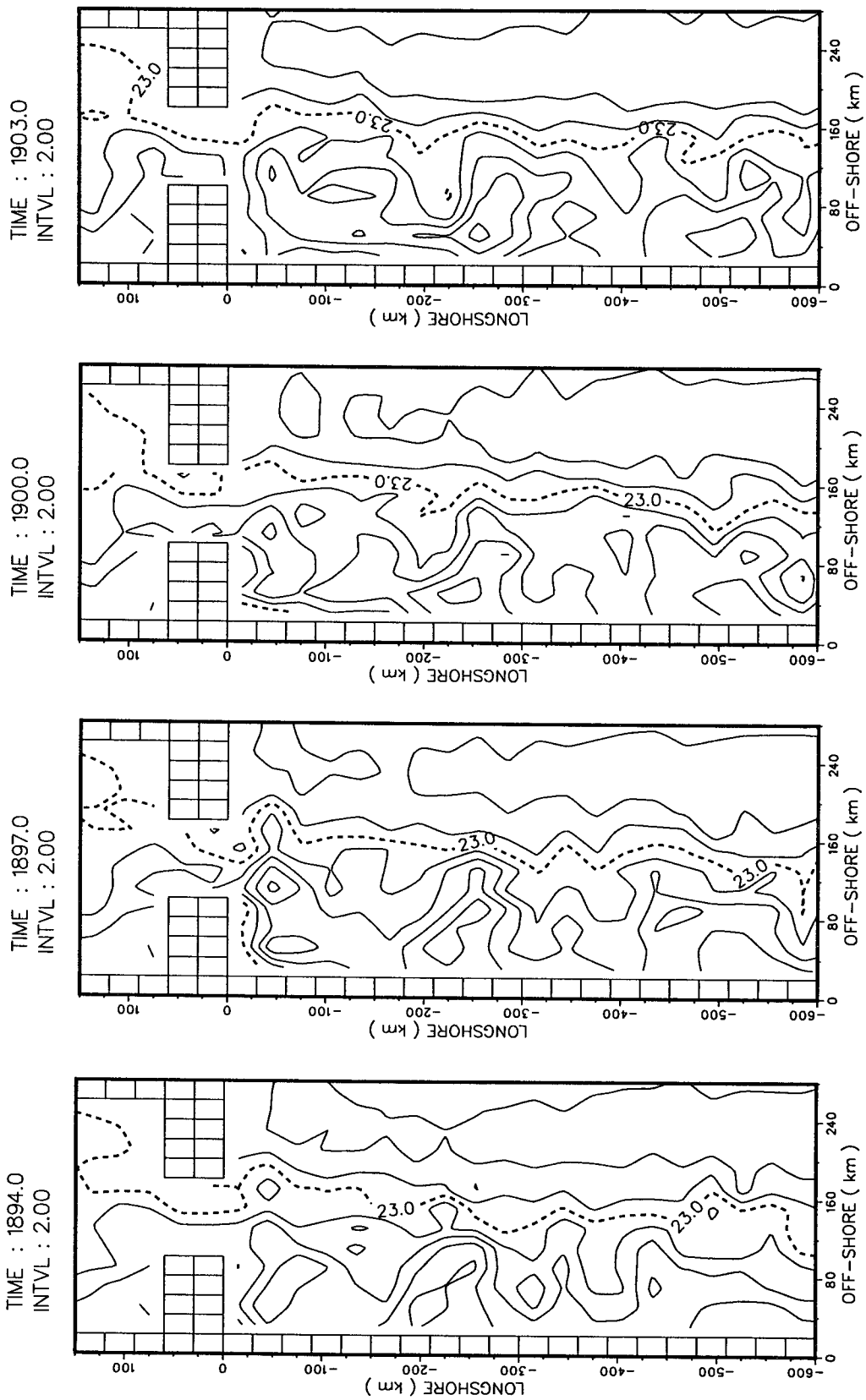

FIG. 9. Experiment *SC*: temperature contours (CI: 2°C) at $z = -30$ m, for (a) $t = 1894$ days, (b) $t = 1897$ days, (c) $t = 1900$ days, and (d) $t = 1903$ days. Thick dashed contour denotes $T = 23$°C.

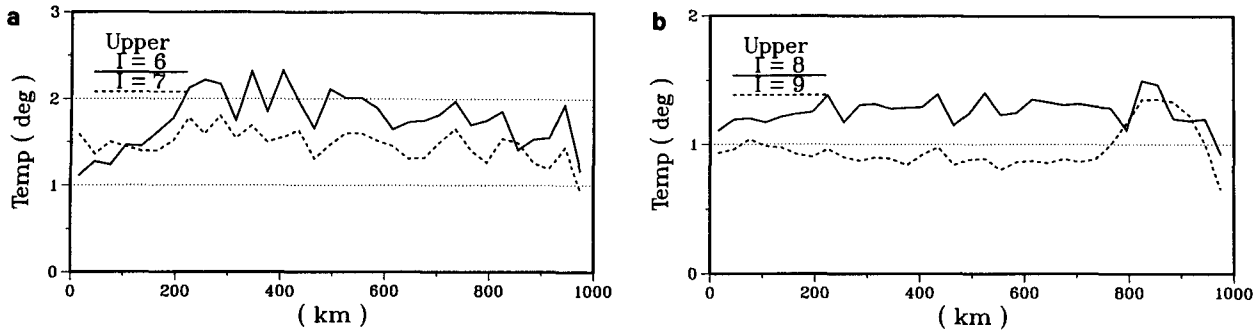

FIG. 10. Experiment *SC*: the standard deviation of temperature averaged over the upper 25 m of the water column as functions of alongshelf distance at (a) two midshelf positions: x = 90 km (solid; local depth = 50 m), and x = 110 km (dash; local depth = 75 m) from the coast; and (b) two outer shelf and shelfbreak positions: x = 130 km (solid; local depth = 100 m), and x = 150 km (dash; local depth = 200 m).

Figure 14 shows near-surface (z = −30 m) temperature contours from t = 1955 days through 1967 days at 4-day intervals, about 100 days after introduction of the flat bottom to the control experiment *SC* at t = 1846 days. These are fairly typical of the temperature distributions found for experiment *SH*, in that they show breaking up of warm eddies in the WBC over the (now flattened) slope south of Kyushu. On examination of 180 days' worth of images, we find a visually higher frequency of eddy breaking in comparison to that for experiment *SC* (cf. Fig. 9), consistent with enhanced baroclinic instability process in experiment *SH*.

The figure also shows an amplifying meander some 200 km upstream of the minibasin, and shoreward intrusions another 200 km farther upstream. These shoreward intrusion locations are about 100 km closer to Kyushu than the corresponding ones for *SC* (compare Figs. 14d and 9d, for example), which suggests that part of the diabathic disturbance source is now due to the minibasin.

c. *The Kyushu shoal experiment, SK*

This case differs from the control experiment, *SC*, in that the shelfbreak and continental slope are more gentle over an area 100 km × 300 km south of Kyushu. This area is shaded in Fig. 2, and the corresponding bottom slope over the bump is shown in Fig. 3b. On the shelfbreak water depth over the bump is about 200–300 m less than the water depth farther south. The WBC is deflected seaward as fluid parcel from the south encounters the bump at 300 km south of Kyushu. Cyclones are constantly produced north of the deflection, and cooler shelf water is drawn offshore. An energy analysis indicates enhanced baroclinic instability over the bump, both because the front is now moved away from the stabilizing influence of the shelfbreak and because the ratio of the upper-layer depth to total water depth increases (Oey 1988). The more gentle topographic slope also tends to destabilize the flow. The cyclone is shown in Fig. 15 with one-year averaged temperature contours at two depths, one averaged over

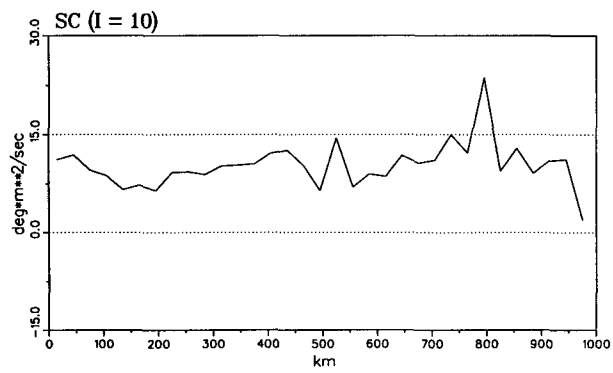

FIG. 11. Experiment *SC*: cross-shelf eddy heat flux, $\int_{-H}^{0} \times (\overline{-u'T'})dz$, at the shelfbreak ($x$ = 170 km from coast; depth = 300 m), as a function of along-shelfbreak distance.

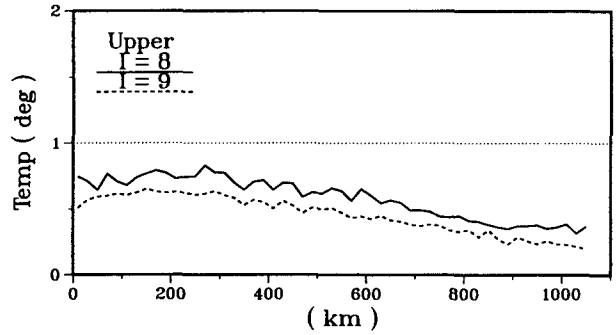

FIG. 12. Experiment *SO*: the standard deviation of temperature averaged over the upper 25 m of the water column as functions of alongshelf distance at two outer shelf and shelfbreak positions: x = 130 km (solid; local depth = 100 m), and x = 150 km (dash; local depth = 200 m) from the coast.

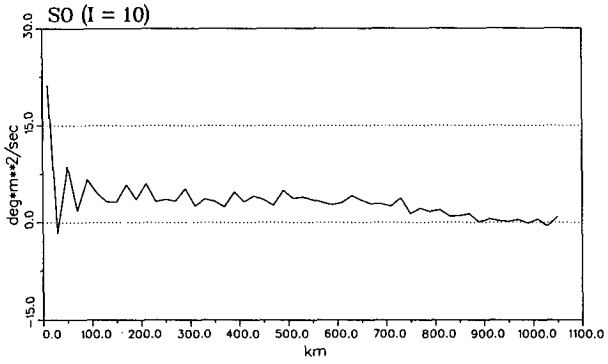

FIG. 13. Experiment *SO*: cross-shelf eddy heat flux, $\int_{-H}^{0} \times (\overline{-u'T'})dz$, at the shelfbreak ($x$ = 170 km from coast; depth = 300 m), as a function of along-shelfbreak distance.

the upper 25 m, and the other one averaged from −25 m to −50 m of the water column. Downstream of the cyclone, shoreward intrusion at the first location of meander resonance, found for the *SC* experiment at about 200 km south of Kyushu, is enhanced; so much that the feature shows up in the mean temperature contour plots. Also seen in these plots is a second location of meander resonance, some 150–200 km upstream of the bump, which probably is caused by the bump acting now as the source of the diabathic disturbance.

5. Volume transports

We now show results that support the hypothesis inferred from observations (see the Introduction) that shelfward deflection of the Kuroshio southwest of Kyushu is not continuous, but rather is made up of cumulative eddies that intrude across the shelfbreak. The *SK* experiment is used here as an example, since its oceanographic setup mimics most closely that in the ECS southwest of Kyushu: the Kuroshio, which is blocked by Kyushu as well as deflected by topographic shoaling southwest of Kyushu.

a. The mean transport field

Figure 16 gives mean transports (Tr_i, i = 1 through 5) across five sections along the shelfbreak, as well as transports through the three straits: the Korea Strait into the northern minibasin (Tr_K), the Taiwan Strait connecting the shelf into the southern minibasin (Tr_T), and the Luzon Strait from the open ocean into the southern minibasin (Tr_L). The Tr_1 represents transport across the shelfbreak bounded by Kyushu to the first standing wave node (about 200 km) south of Kyushu. This is the shelfbreak section across which one sees enhanced shoreward intrusion of eddies. Other shelfbreak sections farther south for Tr_i, i = 2 through 5, are somewhat arbitrarily chosen. The lengths of sections 1 through 3 are each 210 km, that of section 4 is 240 km, and that of section 5 is 120 km. The figure shows that the shelf receives two influx sources in the south, one from the Taiwan Strait (Tr_T), and the other one (Tr_5) is across the shelfbreak just as the WBC enters the open shelf region from the Taiwan eastern outer wall. This second influx is related to enhanced frontal waves formed as the WBC leaves the stabilizing continental slope of Taiwan (cf. Oey 1988). The situation here may also be relevant to the case when the Gulf Stream leaves the Florida Strait into the SAB shelf region (Lee and Atkinson 1983). The sum of Tr_T and Tr_5 is 4.5 Sv. This influx is balanced, however, by outflux across the shelfbreak by $\mathrm{Tr}_2 + \mathrm{Tr}_3 + \mathrm{Tr}_4$, that is, across sections south of the bottom bump, and the model suggests that little of the Tr_T and Tr_5 actually contribute to the Korea Strait transport. This balance is consistent with the northward drop of sea level over the shelf, mentioned earlier with regard to Fig. 5b, which produces offshore transport south of the bump. South of the Charleston Bump in the SAB, recent observations indicate northward drop of sea level consistent with a mean offshore transport of shelf water (Thomas N. Lee, University of Miami, private communication). Thus, the model's mean transport field appears to be quite realistic.

Across the section north of the bump (or, more precisely, north of the steady cyclone in Fig. 15), there is an influx of 4.9 Sv. This is partially balanced by outflux to the south, but most of it is balanced by flow through the Korea Strait, which maintains a mean outflux of 4.3 Sv into the northern minibasin. The transports represented by Tr_1 and Tr_K are not steady, of course, but fluctuate in time with periods of about 10–20 days, as shown next.

b. The unsteady transport

Figure 17 gives time series of the deviations of Tr_1 (dash) and Tr_K (solid); that is, deviations from their respective means shown in Fig. 16. There is some adjustment of the computed field when the bottom bump was introduced. The field nevertheless appears to have settled to a quasi-equilibrium state in about 60 days. The transports vary significantly in time with amplitudes of 1–1.5 Sv and periods of 10–20 days. There is a visual (anti) correlation between the two series, which is readily demonstrated by a correlation analysis. A negative peak in Tr_1, which signifies maximum shoreward intrusion, corresponds with little lag to a positive peak in Tr_K, which signifies maximum outflux into the northern minibasin. The near zero lag suggests a barotropic response. More detailed analyses indicate that Tr_K is not correlated with any of the Tr_i, i = 2 through 5, nor with Tr_T. Thus, transport *variation* through the Korea Strait is strongly affected by episodic eddy intrusions across the shelfbreak from the blocking wall

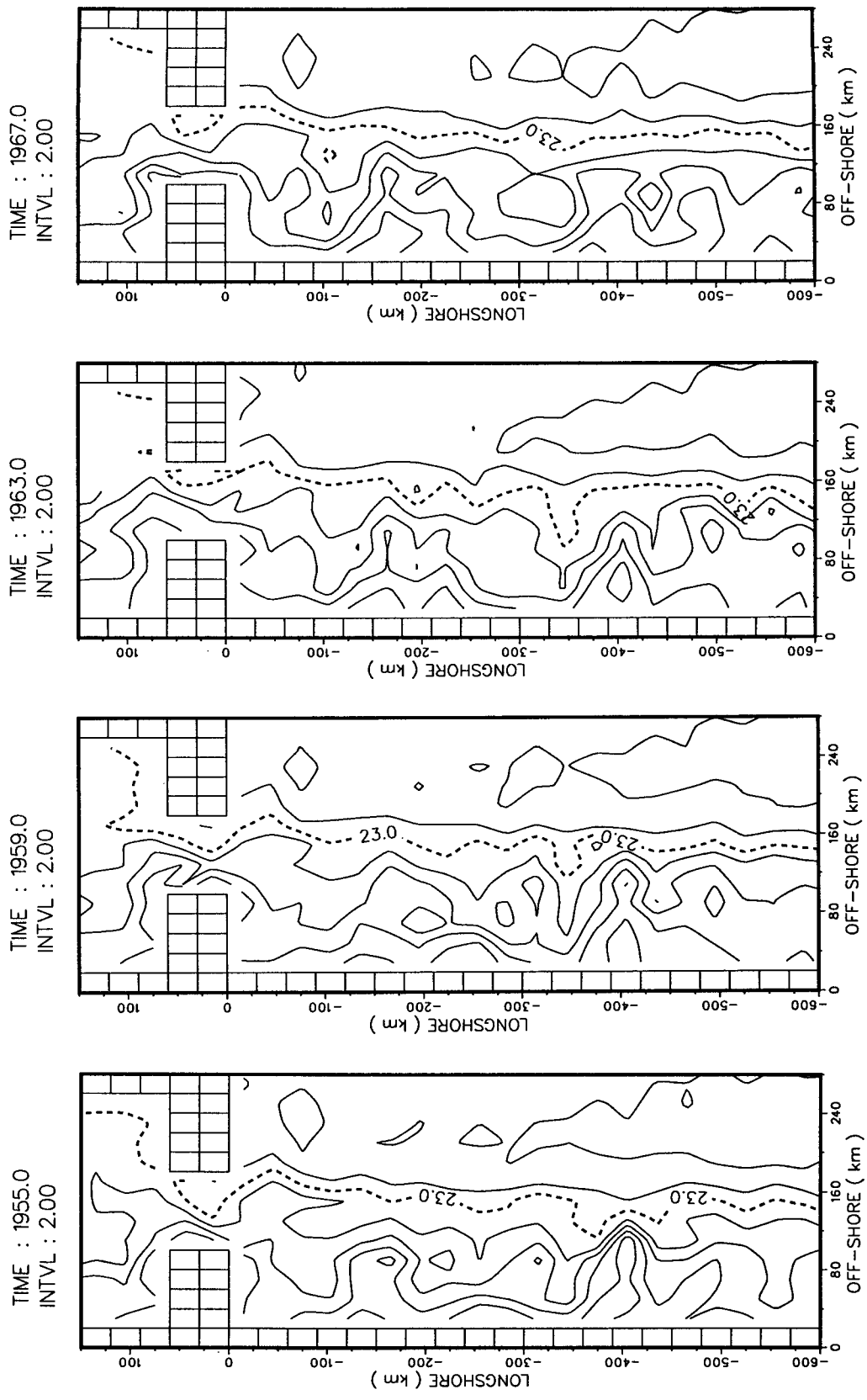

FIG. 14. Experiment *SH*: temperature contours (CI: 2°C) at $z = -30$ m, for (a) $t = 1955$ days, (b) $t = 1959$ days, (c) $t = 1963$ days, and (d) $t = 1967$ days. Thick dashed contour denotes $T = 23$°C.

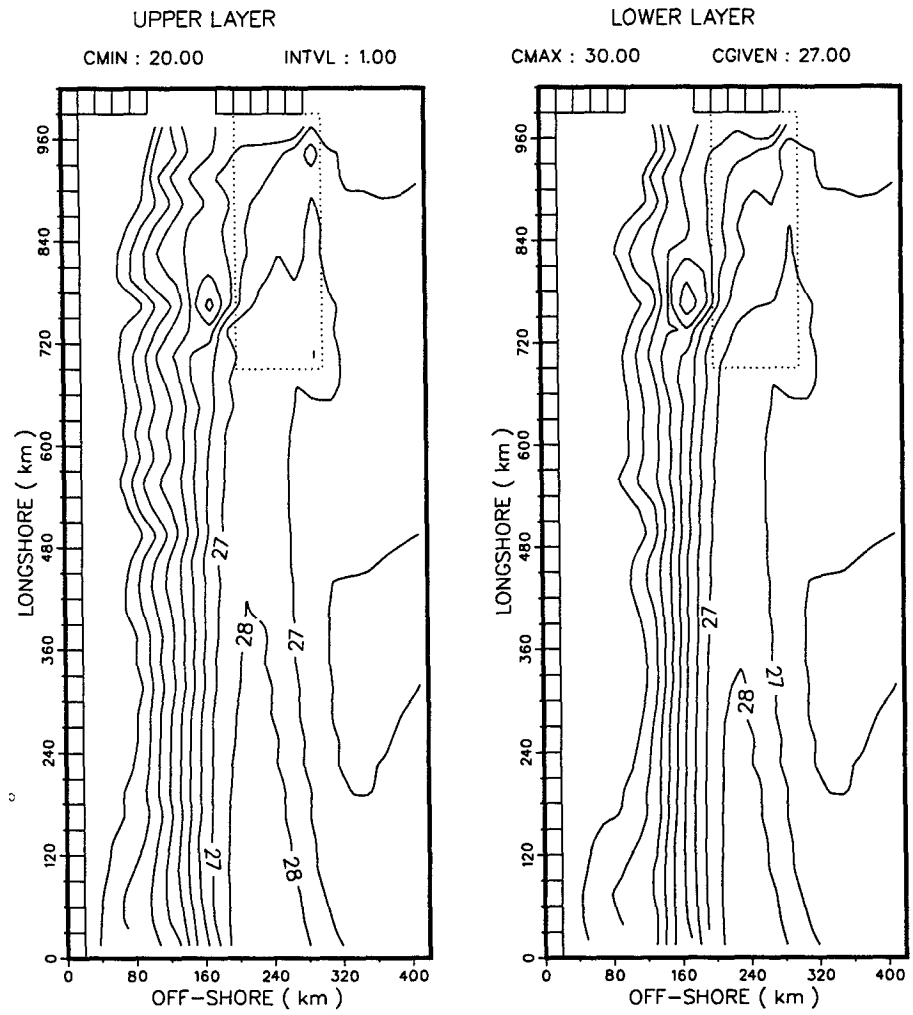

FIG. 15. Experiment *SK*: one-year mean temperature contours averaged (a) from 0 to −25 m, and (b) from −25 to −50 m. The area where the bottom bump is introduced is enclosed by dots.

to the first upstream standing wave node, that is, from Kyushu to about 200 km south of Kyushu.

Figure 18 shows time-sequence contours of temperature at $z = -30$ m, which illustrate one such episodic eddy intrusion event. These start at $t = 2117$ days, 272 days after the introduction of the bump, at 4-day intervals. From Fig. 17 at 272 days, shelfward transport and Korea Strait transport show near local minima (the period that covers the episodic event in Fig. 18 is marked in Fig. 17). This is the beginning of an intrusion event and one sees from Fig. 18a a large shoreward meander (see the $T = 23°C$ contour) located at about 150 to 200 km south of Kyushu. This meander spreads over the shelf (Figs. 18b and 18c) and eventually joins the shelfward intrusion nearer to Kyushu to form a more extensive pool of warm water over the shelf (compare Fig. 18a with 18d). Despite surface cooling, shelf water within the region 200 km south of the Korea Strait, including the strait, warms up during this intrusion phase by about 1.5°C, and the contours make it clear that (as has been checked in a heat-balance calculation) heat flux is across the shelfbreak, not from shelf waters farther south. The sequence also shows that intrusive transport is cumulative in that it is made up of several meander spreadings and eddies. This explains why the period of transport fluctuations in Fig. 17 appears to cover a rather wide range from 10 to 20 days. Near the end of intrusion (Fig. 18d), influx transport across the shelfbreak, Tr_I, and outflux transport through the Korea Strait, Tr_K, both become maxima (Fig. 17).

Observational estimates of the Korea Strait transport vary greatly among investigators and range from 1 to 8 Sv (see references quoted in Moriyasu 1972; Ichiye 1984). There is also a seasonal variation with minimum transport in winter. Results from the present, somewhat

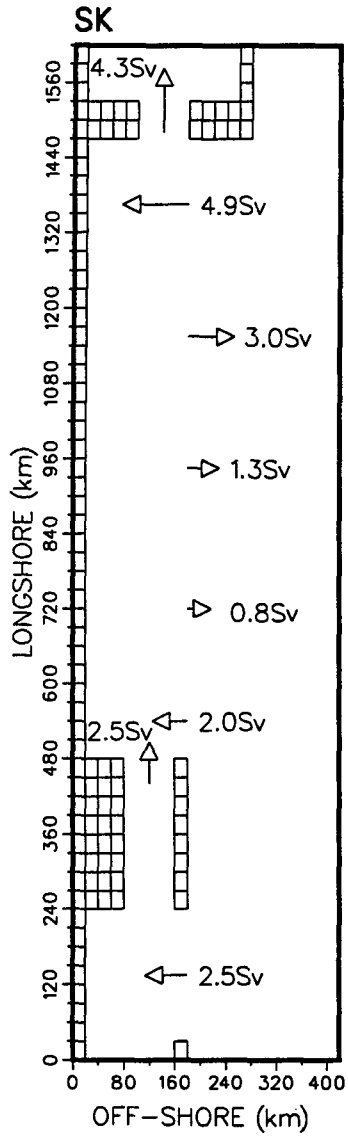

FIG. 16. Experiment *SK*: one-year averaged transports across various sections in the model shelf and local seas.

idealistic, models indicate a mean transport of about 4 Sv, in fair agreement with the observations. Work is currently underway to study effects of wintertime northerly winds, which presumably would modify shelf currents and reduce the transport. The important conclusion obtained from the model is that the Korea Strait transport varies greatly with eddy-intrusive transport across the shelfbreak, and measurements in the Strait must take this variation into consideration.

6. Discussion and summary

This paper describes numerical experiments designed to test the hypothesis that finite-amplitude meanders and shelfward eddy intrusions would occur upstream of a topographic feature as a result of interaction between the blocked standing wave and propagating, small-amplitude frontal waves produced by baroclinic instability process. The model contains three important ingredients of the blocking process: a spunup WBC, the continental slope/shelf, and the blocking island. The identification of sites of large meanders, in the numerical results, along a continental shelfbreak is important for two reasons. These sites are where substantial shoreward heat and mass transports across the shelfbreak can occur and are, therefore, potentially important to the studies of shelf circulation and ecosystem dynamics. Along the ECS shelfbreak, for example, the phenomenon may be relevant to the generation of the Yellow Sea Warm Current (Fig. 1), which has been observed to extend shoreward hundreds of kilometers from the shelfbreak. The water mass of the current consists in part of the warm and saline Kuroshio water (Guan 1983, 1984). The present study suggests that the current can be generated by a series of pinched-off eddies or time-dependent spreadings from large frontal meanders initiated at 200–300 km upstream of the Kyushu Island. For the *SK* experiment, in particular, shelfward transport across the shelfbreak is enhanced northward of the first upstream meander intrusion location. The experiment suggests that here

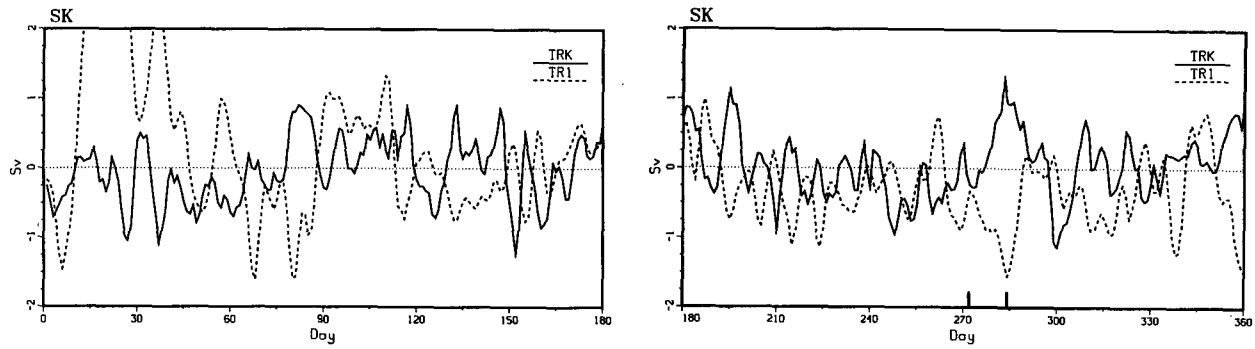

FIG. 17. Experiment *SK*: time variations of transport deviations through the Korea Strait, TR_K (solid), and across the first 200-km section of the shelfbreak south of Kyushu, TR_1 (dash). The time axis is in days starting from the time when the bottom bump south of Kyushu is introduced. Markers at 272 and 284 days enclose periods for which contours in Fig. 18 are plotted.

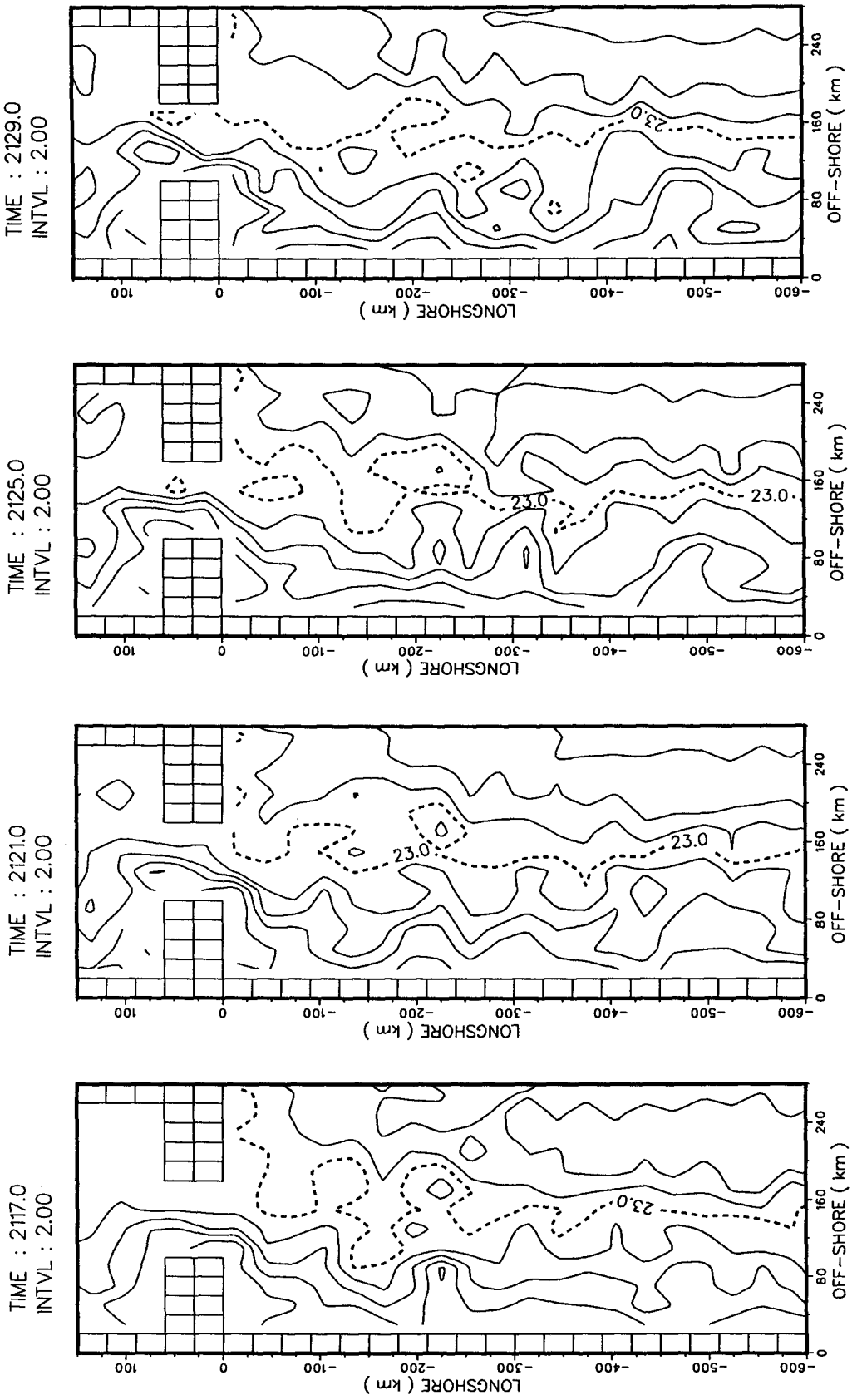

FIG. 18. Experiment *SK*: temperature contours (CI: 2°C) at $z = -30$ m, for (a) $t = 2117$ days (i.e., 272 days after introduction of the bump south of Kyushu), (b) $t = 2121$ days, (c) $t = 2125$ days, and (d) $t = 2129$ days. The thick dashed contour denotes $T = 23$°C. See markers in Fig. 17 for corresponding transport variation during this period.

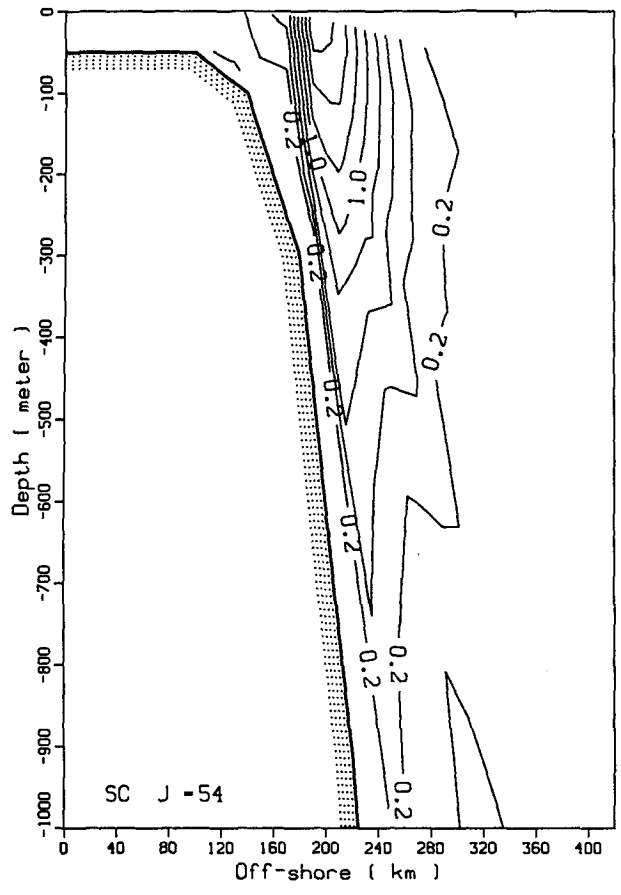
SC J =54
Depth (meter)
Off-shore (km)
0 -100 -200 -300 -400 -500 -600 -700 -800 -900 -1000
0 40 80 120 160 200 240 280 320 360 400
1.0
0.2

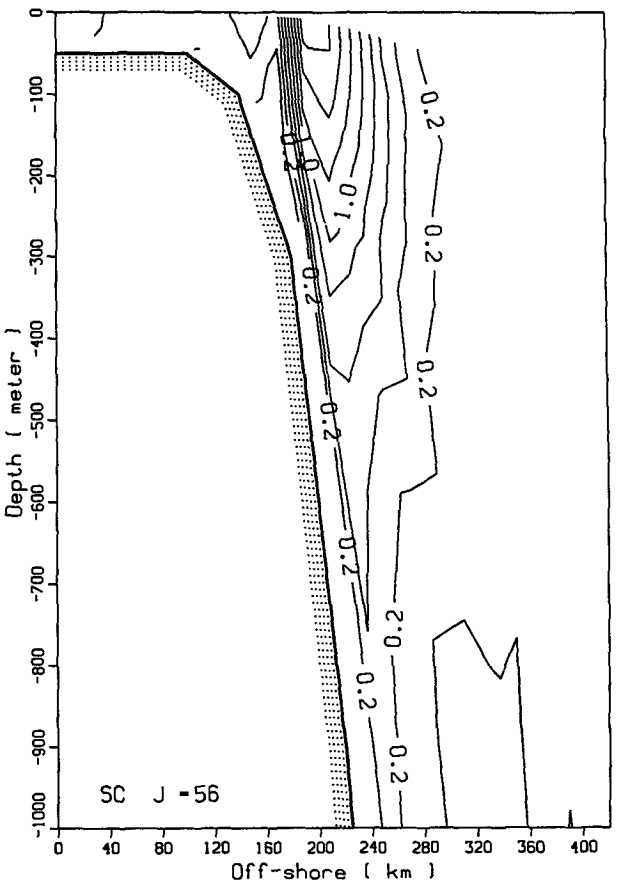
SC J =56
Depth (meter)
Off-shore (km)
0 -100 -200 -300 -400 -500 -600 -700 -800 -900 -1000
0 40 80 120 160 200 240 280 320 360 400
1.0
0.2

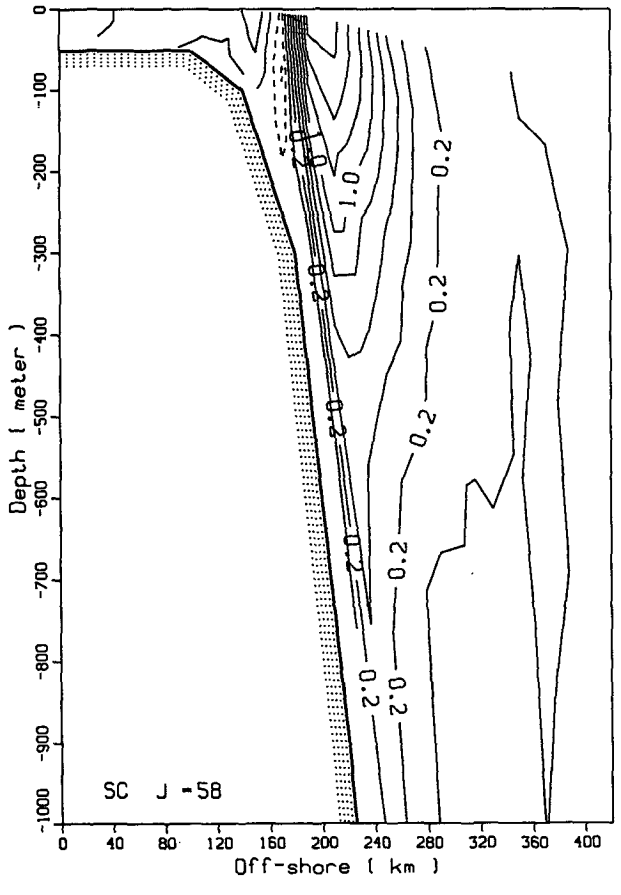
SC J =58
Depth (meter)
Off-shore (km)
0 -100 -200 -300 -400 -500 -600 -700 -800 -900 -1000
0 40 80 120 160 200 240 280 320 360 400
1.0
0.2

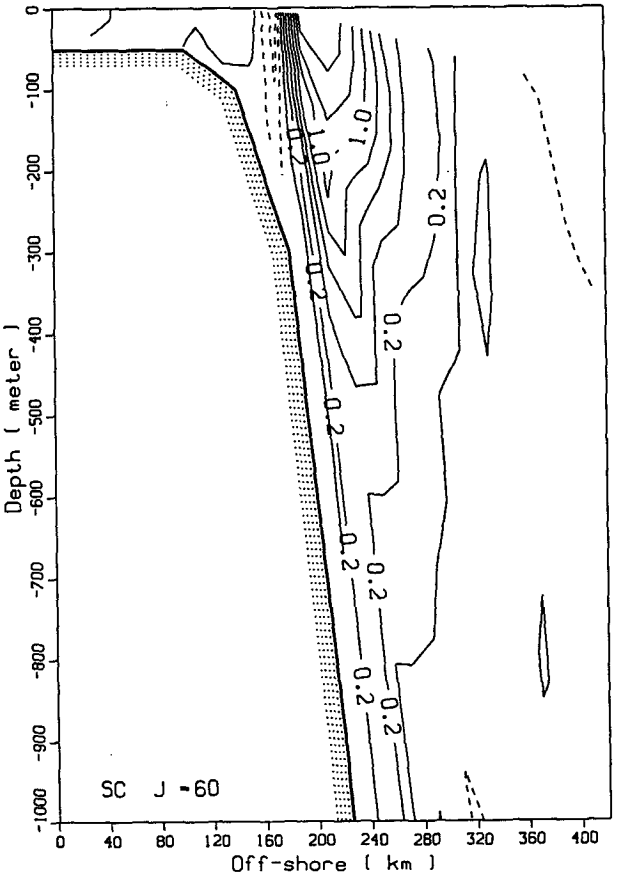
SC J =60
Depth (meter)
Off-shore (km)
0 -100 -200 -300 -400 -500 -600 -700 -800 -900 -1000
0 40 80 120 160 200 240 280 320 360 400
1.0
0.2

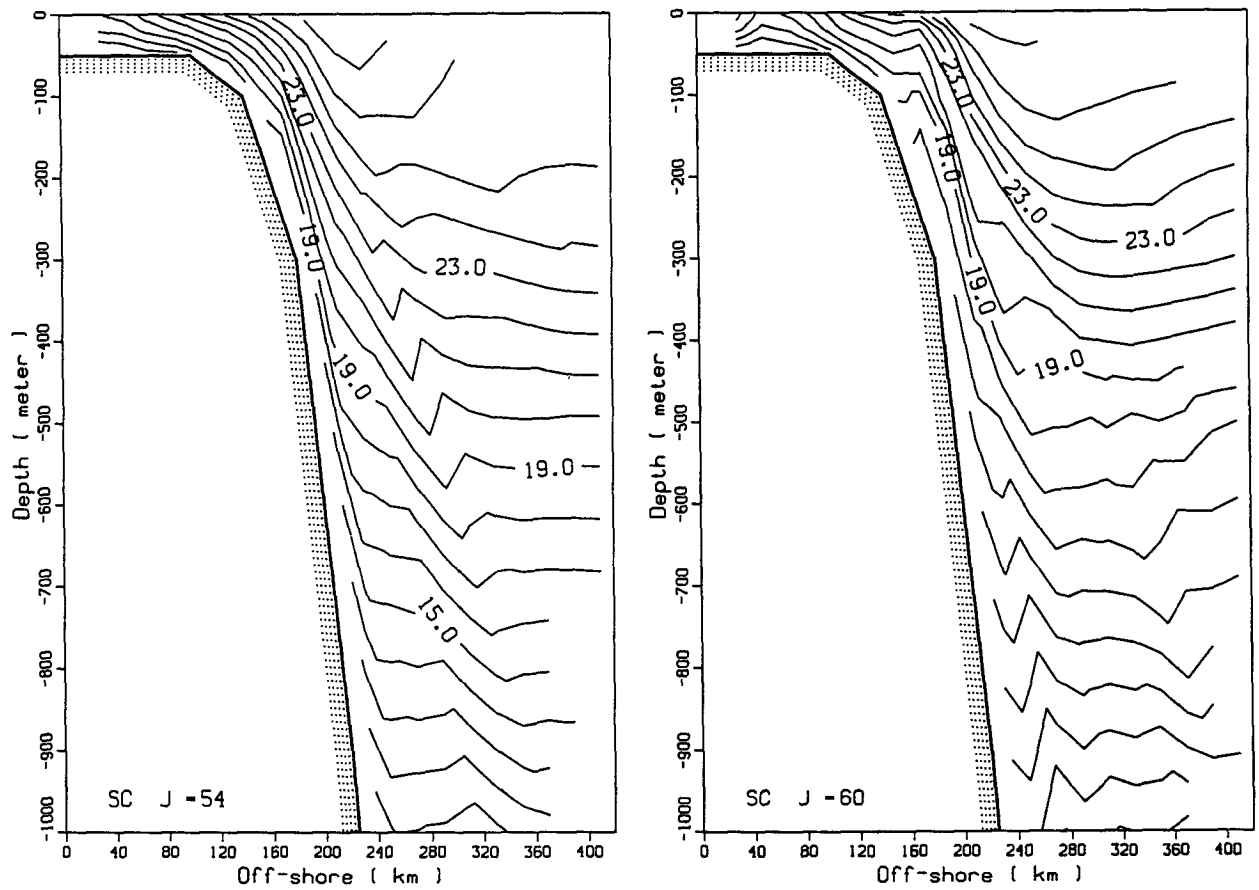

FIG. 20. Experiment *SC*: one-year averaged, cross-shelf section contours of temperature (CI: 1°C), at (a) 270 km (J = 54) and (b) 90 km (J = 60) south of Kyushu.

the Kyushu Shoal plays an important role in setting up strong baroclinic meander that is phase-locked with the lee cyclone. The meander, in turn, produces enhanced shoreward intrusion triggered by the standing wave/meander interaction process. The *SK* experiment gives a one-year averaged intrusive transport of about 0.3 Sv at the first upstream meander location, a substantial but not inconceivable number. Because of the model geometry, the shelf circulation, which results from this intrusion, is of course not modeled. The point is that we have shown a mechanism by which large amounts of WBC water can intrude onto the continental shelf, without resort to wind or other forcing over the shelf. It is noteworthy that the Yellow Sea warm current, at least near the bottom, exists irrespective of seasons (Guan 1983, 1984), which suggests that its generation must be fundamentally related to the dynamics of the Kuroshio branching, described here, rather than to winds or tides.

Second, these sites are sources of frontal instability. In Fig. 12, for experiment *SO*, the intensity of the mean-squared temperature fluctuation is about half of that for experiment *SC* in Fig. 10. Also, the (along-shelfbreak) distribution is almost white, which suggests that whatever meanders that may be generated by dynamical instability simply propagate along the WBC front, and there are no site-specific sources. Thus, the phenomenon offers a mechanism for an otherwise "quiet" WBC along a stabilizing continental slope margin to become unstable and develop meanders. Of course we have only demonstrated this for the special case for which an island was a primary diabathic source of disturbance. We did find, however, that a "canyon" (the northern minibasin, experiment *SH*) or a shoal

FIG. 19. Experiment *SC*: one-year averaged, cross-shelf section contours of alongfront velocity (CI: 0.2 m s^{-1}, negative values are dashed), at (a) 270 km (J = 54), (b) 210 km (J = 56), (c) 150 km (J = 58), and (d) 90 km (J = 60) south of Kyushu.

(experiment *SK*) can also serve as the diabathic source of disturbance.

The existence of this instability source, and the resulting increased eddy activity caused by it, can be seen from alongfront velocity across the first upstream standing wave node, located at about 200 km south of Kyushu. Oey (1988) has shown that increased baroclinic instability produces current branchings around meander cyclones. Thus, one expects current branchings downstream of the node where enhanced meanders occur, and their cumulative effects must show up in the mean field also. Figure 19 shows one-year averaged, cross-shelf section contours of the alongfront velocity, for experiment *SC*, at 270 km (Fig. 19a, J = 54), 210 km (Fig. 19b, J = 56), 150 km (Fig. 19c, J = 58), and 90 km (Fig. 19d, J = 60) south of Kyushu. The four profiles are similar in the main WBC region over the slope. Over the shelfbreak, the contours show positive alongfront flow for locations upstream of the node (Figs. 19a and 19b), while some regions are negative (dashed) throughout the water column for locations downstream of the node, Figs. 19c and 19d. The alongfront flow therefore branches as it crosses the node at about 200 km south of Kyushu, and the branching actually exists at all grid points from 30 to 180 km south of Kyushu. The inshore component of the branched currents of course contributes to the net intrusive transport shoreward. Upwellings associated with cyclones exist between the two branched currents, as illustrated in Fig. 20, which gives the mean temperature contour plots corresponding to Figs. 19a and 19d. For the section downstream of the node (Fig. 20b), one sees uplifted temperature contours over the shelfbreak. Features similar to Figs. 19 and 20 are found also for experiments *SH* and *SK*. In the latter, in particular, branching is enhanced by the bump (cf. Fig. 15).

Because of this instability source, the portion of shelfbreak front downstream of the source is often eroded by eddies so that shelfward transport across the shelfbreak varies in time. We showed that flow across the ~200 km stretch of the shelfbreak south of Kyushu is made up of eddies, which intrude shoreward, and that the resulting transport correlates well with transport through the Korea Strait. This result supports the hypothesis, referred to in the Introduction, that the Tsushima Current is generated by cumulative eddy intrusions across the shelfbreak southwest of Kyushu.

Our future work will include seamounts instead of islands as the diabathic disturbance sources (Oey et al. 1991). We will study effects of wind forcing, as well as effects of various shelf conditions (stratification, for example) on the intensity of WBC/shelf interaction. A study of what dynamics is involved as the WBC water intrudes across a finite extent of the shelfbreak onto the shelf will also be of interest, as analogies and contrasts may be usefully drawn between this and the intrusion of buoyant water from wide estuaries onto the continental shelf. Finally, we will study the influence of a meandering WBC on nearshore circulations induced, for example, by riverine discharge and/or winds.

Acknowledgments. We thank the reviewers for their constructive comments and criticisms. We thank the Stevens Institute of Technology computer center for graphics supports. Chisato Mizutani typed the manuscript. We are grateful to supports by the National Science Foundation, under Grant OCE-8711614. The support of the National Center for Supercomputing Applications, Urbana–Champaign, Illinois, where the calculations reported herein were completed, are also gratefully acknowledged.

REFERENCES

Atkinson, L. P., E. Oka, S. Y. Wu, T. J. Berger, J. O. Blanton and T. N. Lee, 1989: Hydrographic variability of southeastern U.S. shelf and slope waters during the Genesis of Atlantic Lows Experiment: Winter, 1986. *J. Geophys. Res.*, **94,** 10 699–10 713.

Bane, J. M., Jr., 1983: Initial observations of the subsurface structure and short-term variability of the seaward deflection of the Gulf Stream off Charleston, South Carolina. *J. Geophys. Res.*, **88,** 4673–4684.

Blanton, J. O., L.-Y. Oey, J. Amft and T. N. Lee, 1989: Advection of momentum and buoyancy in a coastal frontal zone. *J. Phys. Oceanogr.*, **19,** 98–115.

Blumberg, A. F., and G. L. Mellor, 1983: Diagnostic and prognostic numerical circulation studies of the South Atlantic Bight. *J. Geophys. Res.*, **88,** 4579–4592.

Chao, S.-Y., and T. W. Kao, 1987: Frontal instabilities of baroclinic ocean currents with applications to the Gulf Stream. *J. Phys. Oceanogr.*, **17,** 792–807.

——, and T. W. Kao, 1989: Jet bifurcation in the lee of obstacles, 42 pp.

Guan, B., 1983: A sketch of the current structures and eddy characteristics in the east China Sea. *Proc. of the Int. Symp. on Sedimentation on the Continental Shelf with Special Reference to the East China Sea,* Hangzhou, China, 1–9.

——, 1984: Major features of the shallow water hydrography in the east China Sea and Huanghai Sea. *Ocean Hydrodynamics of the Japan and East China Sea,* T. Ichiye, Ed., Elsevier, 1–13.

Huh, O. K., 1982: Spring seasonal flow of the Tsushima Current and its separation from the Kuroshio: Satellite evidence. *J. Geophys. Res.*, **87,** 9687–9693.

Ichiye, T., 1984: Some problems of circulation and hydrography of the Japan Sea and the Tsushima Current. *Ocean Hydrodynamics of the Japan and East China Sea,* T. Ichiye, Ed., Elsevier, 15–54.

Lee, T. N., and L. P. Atkinson, 1983: Low-frequency current and temperature variability from Gulf Stream frontal eddies and atmospheric forcing along the southeast United States outer continental shelf. *J. Geophys. Res.*, **88,** 4541–4567.

——, and E. Waddell, 1983: On Gulf Stream variability and meanders over the Blake Plateau at 30°N. *J. Geophys. Res.*, **88,** 4617–4631.

Miita, T., and K. Kawatate, 1986: Trajectories of drift bottles released in the Tsushima Strait. *Progress in Oceanography,* Vol. 17, Pergamon, 255–263.

Moriyasu, S., 1972: The Tsushima Current. *Kuroshio,* H. Stommel, and K. Yoshida, Eds., University of Washington Press, 353–369.

Muneyama, K., Y. Asanuma, Y. Sasaki, S. Saitho, Y. Tozawa and T. Ichiye, 1984: An application of NOAA AVHRR for oceanography in the east China Sea. *Ocean Hydrodynamics of the Japan and East China Sea,* T. Ichiye, Ed., Elsevier, Oceanogr. Ser., **39,** 375–386.

Nitani, H., 1972: Beginning of the Kuroshio. *Kuroshio,* H. Stommel, and K. Yoshida, Eds., University of Washington Press, 129–163.

Oey, L.-Y., 1986: The formation and maintenance of density fronts on United States southeastern continental shelf during winter. *J. Phys. Oceanogr.,* **16,** 1121–1135.

——, 1988: A model of Gulf Stream frontal instabilities, meanders, and eddies along the continental slope. *J. Phys. Oceanogr.,* **18,** 211–229.

——, G. L. Mellor and R. I. Hires, 1985: A three-dimensional simulation of the Hudson–Raritan estuary. Part I: Description of the model and model simulations. *J. Phys. Oceanogr.,* **15,** 1676–1692.

——, L. P. Atkinson and J. O. Blanton, 1987: Shoreward intrusions of upper Gulf Stream water onto the United States southeastern continental shelf. *J. Phys. Oceanogr.,* **17,** 2318–2333.

——, T. Ezer, G. L. Mellor, and P. Chen, 1991: A model study of bump-induced western boundary current variabilities. *28th Int. Liege Colloq. on Ocean Dynamics,* Belgium. Submitted to the Colloq. issue of the J. Mar. Sys.

Orlanski, I., and M. D. Cox, 1973: Baroclinic instability in ocean currents. *Geophys. Fluid Dyn.,* **4,** 297–332.

Pedlosky, J., 1979: *Geophysical Fluid Dynamics.* Springer-Verlag, 624 pp.

Richardson, W. S., W. J. Schmitz, Jr. and P. P. Niiler, 1969: The velocity structure of the Florida Current from the Straits of Florida to Cape Fear. *Deep-Sea Res.,* **16,** 225–231.

Shaw, P.-T., 1989: The intrusion of water masses into the sea southwest of Taiwan. *J. Geophys. Res.,* **94,** 18 213–18 226.

Sugimoto, T., S. Kimura and K. Miyaji, 1988: Meander of the Kuroshio front and current variability in the east China Sea. *J. Oceanogr. Soc. Japan,* **44,** 125–135.

Thompson, J. D. and W. J. Schmitz, 1989: A limited-area model of the Gulf Stream: Design, initial experiments, and model–data intercomparison. *J. Phys. Oceanogr.,* **19,** 791–814.

Worthington, L. V., and H. Kawai, 1972: Comparison between deep sections across the Kuroshio and the Florida Current and the Gulf Stream. *Kuroshio.* H. Stommel, and K. Yoshida, Eds., University of Washington Press, 371–385.